HHS Public Access

Author manuscript

IEEE Trans Biomed Eng. Author manuscript; available in PMC 2020 May 01.

Published in final edited form as:

IEEE Trans Biomed Eng. 2019 May ; 66(5): 1231–1241. doi:10.1109/TBME.2018.2871415.

Epilepsy-on-a-chip System for Antiepileptic Drug Discovery

Jing Liu [Member IEEE],
Department of Electrical and Computer Engineering, Lehigh University, Bethlehem, PA, USA. She is now with University of California, San Francisco, CA, USA.

Anna R. Sternberg,
IDEAS Program, Lehigh University, Bethlehem, PA, USA. She is now with Georgetown University, Washington D.C., USA.

Shabnam Ghiasvand [Member IEE], and
Department of Bioengineering, Lehigh University, Bethlehem, PA, USA.

Yevgeny Berdichevsky* **[Member IEEE]**
Department of Electrical and Computer Engineering and Department of Bioengineering, Lehigh University, Bethlehem, PA, USA

Abstract

Objective: Hippocampal slice cultures spontaneously develop chronic epilepsy several days after slicing and are used as an in vitro model of post-traumatic epilepsy. Here, we describe a hybrid microfluidic-microelectrode array (μflow-MEA) technology that incorporates microfluidic perfusion network and electrodes into a miniaturized device for hippocampal slice culture based antiepileptic drug discovery.

Methods: Field potential simulation was conducted to help optimize the electrode design to detect seizure-like population activity. Epilepsy-on-a-chip model was validated by chronic electrical recording, neuronal survival quantification, and anticonvulsant test. To demonstrate the application of μflow-MEA in drug discovery, we utilized a two-stage screening platform to identify potential targets for antiepileptic drugs. In Stage I, lactate and lactate dehydrogenase biomarker assays were performed to identify potential drug candidates. In Stage II, candidate compounds were retested with μflow-MEA based chronic electrical assay to provide electrophysiological confirmation of biomarker results.

Results and Conclusion: We screened 12 receptor tyrosine kinases inhibitors, and EGFR/ErbB-2 inhibitor and cFMS inhibitor were identified as novel antiepileptic compounds.

Significance: This epilepsy-on-a-chip system provides the means for rapid dissection of complex signaling pathways in epileptogenesis, paving the way for high-throughput antiepileptic drug discovery.

*correspondence berdichevsky@lehigh.edu.

Index Terms—

brain slices; drug discovery; electrophysiology; epilepsy; MEA; microfluidics; neural

I. Introduction

Currently available antiepileptic drugs require continuous administration to suppress seizures, and there is no therapy available in clinic to prevent the development of epilepsy (epileptogenesis) [1]. Organotypic hippocampal cultures have been increasingly used as an in vitro model of post-traumatic epilepsy. These cultures spontaneously develop seizures about one week after dissection [2]–[4]. Epileptogenesis in this model has a compressed timescale and can be monitored with chronic imaging, electrical recording, or by detecting biochemical markers of seizures [3], [5]–[7]. Organotypic hippocampal cultures thus provide an easy-to-access in vitro model for antiepileptic drug discovery [5]–[10].

Determination of antiepileptic properties of a compound in organotypic hippocampal culture model of epilepsy requires at least two weeks of chronic electrical[3] or optical[5] recordings or observation via biomarker sampling [6], [7]. Of these methods, only biomarker sampling enables sufficient experimental throughput to screen a library of 100 or more compounds [7]. Since biomarkers do not represent direct measurements of parameters such as number or duration of seizures, second stage of screening using electrical recordings is necessary to confirm “hits”. Microelectrode array (MEA) technology provides highly sensitive recordings and supports chronic recordings in organotypic brain slice cultures over several weeks [11]–[18]. However, typical MEA devices are designed to support only one brain slice culture, due to the low scalability of organotypic culture chamber. This limits applicability of typical MEAs to screens using organotypic hippocampal culture model of epilepsy. Our previously developed perfused drop technique can highly increase the throughput of organotypic culture experiments [19]. In this technique, hippocampal slice was maintained on a glass substrate in a medium drop confined by a polydimethylsiloxane (PDMS) culture well. Drops were continuously perfused with culture medium through photolithographically defined microchannel network. Perfused drop device could support organotypic slice cultures for over 2 weeks, and was compatible with planar MEAs. Here, we describe a novel hybrid microfluidic-MEA (μflow-MEA) device that extends perfused drop technique to support 6 organotypic cultures on a single chip. μflow-MEA device features new, simplified large area strip electrodes optimized for detection of electrographic seizures in 6 separate perfused drops. The new μflow-MEA is capable of chronic recording from 6 cultures simultaneously. This is particularly important for screening experiments since μflow-MEA enables monitoring of the experimental replicates and controls on the same chip to reduce variability.

To demonstrate how this device can facilitate antiepileptic drug discovery, we conducted a pilot screen of small molecule inhibitors of receptor tyrosine kinases (RTKs). Many of RTKs are expressed in the hippocampus [20] and are altered by brain injury [21]–[27], the most common known cause of acquired epilepsy [28], [29]. We present a two-stage screening platform based on organotypic hippocampal cultures model of epilepsy. In the first stage,

epileptogenesis during chronic RTK inhibitor application was evaluated by lactate and lactate dehydrogenase (LDH) levels, biomarkers of seizure-like activity and seizure-dependent cell death, respectively [3], [6], [7]. In the second stage, μflow-MEA-based chronic electrical assay was used to verify results obtained in the first stage.

II. Results

A Device design and simulation

The device has 8 metal strip electrodes (30 μm × 3 mm) recording from 6 culture wells (diameter = 6 mm), with one electrode for each well, and one additional electrode in two wells (since we used a 16 channel data acquisition system, 8 channels were allocated to each device), and a reference electrode (diameter = 3 mm) in the fluid reservoir (Fig. 1; Supplementary Fig. S1). PDMS microfluidic system was bonded to metal patterned MEA.

In our simplified MEA design, the portion of the recording electrode in the organotypic culture well was left uninsulated. Increased electrode area reduces electrical noise, but also moderates detection sensitivity by averaging out field potentials occurring over the length of electrode. Unlike standard electrophysiology platforms where the brain slice is placed in a large chamber (~30 mm diameter, containing 1~2 ml of conducting medium), μflow-MEA records from cultures that are physically confined in PDMS mini well (6 mm diameter, containing 5~10 μl conducting medium). We found that electrical signal attenuation due to increasing distance between signal source and recording electrode is highly reduced in a 6 mm culture well compared to a standard 35 mm culture dish [Supplementary Fig. S2(a)]. This partially offsets the loss of detection sensitivity due to large electrode area (signal recorded by a large strip electrode is only ~40–50% lower than signal recorded by a point microelectrode in a 6 mm well [Supplementary Fig. S2(b)]). This offset is not sufficient to use large strip electrodes to record signals from small dipoles such as multiple neurons [Supplementary Fig. S3, discussed in more detail below]. However, seizure activity is characterized by highly synchronous neuronal firing which may further offset signal loss due to potential averaging over large electrode area. To test this hypothesis, we built a current source model of seizure-like activity in hippocampal slice culture [Fig. 2]. Anatomy of the hippocampal slice is defined by multiple layers: stratum oriens (*o*) is where the basal dendrites of pyramidal neurons (the principal excitatory neurons of the hippocampus) are located; pyramidal layer (*p*) contains the cell body (soma) of pyramidal neurons; stratum radiatum (*r*) contains apical dendrites of pyramidal neurons; stratum lacunosum-moleculare (*lm*) also contains apical dendrites of pyramidal neurons; dentate molecular layer (*m*) contains dendrites of the dentate granule cells; granule cell layer (*g*) contains cell bodies of the dentate granule cells. Layers can be observed in a confocal image of NeuN staining [Fig. 2(a)]. When spontaneous synchronized activity involves the whole hippocampus, and at the moment that dendrites are depolarized by excitatory inputs, current sink forms in the layers that contain dendrites (*o*, *r*, *m*). Correspondingly, current source forms in the layers that contain cell bodies (*p*, *g*, *CA3p*). Conversely, when neurons are firing action potentials, current sink forms in soma layers, and current source forms in dendrite layers. Therefore, during dynamic activity, the current sink-source pattern will flip over the time [30], [31]. The current sink-source pattern of epileptiform activity in a hippocampal slice has been

observed in previous work [11], [32]–[34]. Based on these data, we created a current source model of seizure-like activity that involves the whole slice [Fig. 2(b)]. Current sink forms in *o*, *r*, *m* layers, and current source forms in *p*, *lm*, *g*, *CA3p* layers. The current source in *lm* layer is due to the formation of current quadrupoles in CA1 pyramidal neurons [31]. We simulated the field potential in mini culture well (diameter = 6 mm, fluid depth = 100 μm), and field potential in standard petri dish (diameter = 35 mm, fluid depth = 2 mm), which mimics the widely used submerged slice chamber [35], [36] [Fig. 2(c)]. The field potential distribution in the plane of well floor is shown in Fig. 2(d). The plot of field potential distribution along the x=0 and y=0 axis showed that the electrical field due to synchronized activity is highly amplified in mini well compared with field in standard well [Fig. 2(e)].

We then calculated the potential amplitude that can be detected by uninsulated electrodes placed at different positions in the culture well. Field potential distribution along the length of the electrodes and the corresponding average potential of each electrode position are shown in Fig. 3(a)–(c). The electrodes are predicted to detect field potential ranging from 0.2 mV to 2.5 mV, which is similar to previously observed potential amplitude of epileptiform activity in brain slices [37]–[39]. A current dipole model was built to simulate multiple neuron activity (multiunit activity). The results are shown in Supplementary Fig. S3. Electrodes placed in the vicinity of the current dipole are predicted to detect field potential ranging from 0.2 μV to 1.8 μV, which is below the system noise level (about 10 μV). Therefore, uninsulated strip electrodes lack the sensitivity to detect multiunit activity.

Simulations and experiments demonstrated that field potential is amplified in spatially confined mini culture well, which offsets the loss of sensitivity caused by increased electrode area. The uninsulated strip electrode is sensitive to seizure-like activity in hippocampal slice culture, but filters out regular multiunit activity, simplifying automatic seizure detection. In experiments, we found that seizures recorded by large strip electrodes have similar amplitudes, but lower baseline variation compared to seizures recorded by tungsten microelectrodes (point electrode), and the signal to noise ratio (SNR) of strip electrodes is slightly lower than that of point electrodes [Fig. 3 (d); $p < 0.001$, student *t* test, n = 6 electrodes for each type].

B. Validation of in vitro model of epileptogenesis on μflow-MEA

We developed a system capable of operating two μflow-MEA devices with a 16-channel data acquisition [Fig. 1(c)]. We then carried out validation experiments described in this sub-section to confirm that organotypic hippocampal cultures maintained on multi-slice, integrated μflow-MEA device behave in the same way as when maintained on rocking plates or in a single perfused drop. In other words, we verified that epilepsy modeling aspects of organotypic hippocampal cultures (appearance of spontaneous seizures after a latent period and response to antiepileptic drug) were not lost due to change in culture method or increased density of slices on a single chip.

We evaluated the culture viability in μflow-MEA devices by counting the number of surviving neurons at 14 days in vitro (DIV), and compared perfused cultures (μflow-MEA) and control cultures generated via the interface method that was used for this epilepsy model in previous work [4, 7]. Confocal imaging of NeuN staining showed similar well maintained

cytoarchitecture and densely packed neurons in perfused and control cultures [Fig. 4(a)]. Neuron counts showed no difference between control and perfused cultures in CA3c, CA3b and CA1 subregions [Fig. 4(b); p = 0.366, 0.491, and 0.289, respectively, student t test, n = 9 each condition]. This result confirmed that microfluidic perfusion and chronic electrophysiology do not compromise viability of organotypic cultures.

Continuous electrical recording was conducted from 3 DIV to 14 DIV. Raster plots were generated from electrical data with interictal and ictal (seizure) events color-coded based on paroxysmal event frequency. [Fig. 4(c)], as described previously [3, 6, 19]. The chronic data revealed epileptogenesis in organotypic cultures on μflow-MEA: a latent period after dissection, then spontaneous appearance of interictal and ictal events which continued in the later period. The incidence of interictal and ictal activity progressively increased with the age of cultures [Fig. 4(d); n = 36 cultures, from 10 animals]. The time course of epileptogenesis was consistent with previous observations in organotypic hippocampal cultures maintained on rocking plates [2], [3], [5], [6] and in perfused drops [19].

We tested the effect of phenytoin, a first-line anticonvulsant that is used to treat epilepsy in human patients, on hippocampal cultures maintained on μflow-MEA. Seizure-like activity was transiently abolished when phenytoin was applied and rebounded after the termination of drug application [Fig. 4(e),(f); n = 3]. Thus, phenytoin exerted acute, reversible anticonvulsive effects on this model, which is consistent with previous findings [3].

C. Chronic screen of receptor tyrosine kinase (RTK) inhibitors

Short-term neurotoxicity pre-screen (0–7 DIV) was conducted to determine the maximum non-toxic concentrations of each inhibitor. These concentrations were then applied to cultures for chronic screen in Stage I (lactate and LDH assay), and Stage II (chronic electrical assay). Concentrations used for each inhibitor are indicated in Supplementary Table SI.

In Stage I, we screened 12 hippocampal RTK inhibitors listed in Supplementary Table SI. We integrated the lactate and LDH production of inhibitor-treated cultures between 3 and 14 DIV, and normalized it to vehicle-treated control (n = 3 cultures, from the same animal). A scatter plot of lactate versus LDH is shown in Fig. 5(a) for individual cultures. Some lactate and LDH values were lower than the mean of controls by more than 3 times the mean standard derivation (data points that are outside the dashed circle), suggesting antiepileptic effect. p values of LDH and lactate assays are listed in Supplementary Table SI. Significantly lower lactate and LDH were observed for cultures treated with VEGF inhibitor II, PDGF inhibitor III, and VEGF inhibitor IV. Cultures treated with GTP-14564 (multi-target inhibitor for c-fms, c-kit and Flt-3), EGFR/ErbB-2 inhibitor, and Flt-3 inhibitor III showed significantly lower lactate. Cultures treated with AG 1259 (PDGF inhibitor), VEGFR2 inhibitor II, and cFMS inhibitor showed significantly lower LDH (one-way ANOVA with Holm-Sidak post hoc analysis, n = 3 cultures each condition).

In Stage II, a chronic electrical assay was conducted to verify the results obtained in Stage I. As is shown in Fig. 1(c), two μflow-MEA chips were used to test 3 drug-treated conditions with one vehicle-treated control in a single experiment (n = 3 cultures each condition,

cultures were from the same animal). Chronic recording was initiated on 1 DIV and continued until14 DIV. Drugs and vehicle were applied from 3 DIV. A representative 1 hour recording on 7 DIV in 12 cultures from one experiment is presented in Fig. 5(b). Aurora inhibitor II (1 μM), which showed no antiepileptic effect in our test screen, was screened in addition to 12 RTKs from Stage I. Significant antiepileptic effect was revealed for EGFR/ErbB-2 and cFMS inhibitors [Fig. 5(c)–(g)]. Cumulative time seizing and cumulative number of seizures were normalized to the total time seizing and total number of seizures of vehicle-treated control cultures, respectively, and are shown in Fig. 5(d) and (e). EGFR/ErbB-2 inhibitor-treated and cFMS inhibitor-treated cultures showed significant decrease in cumulative distribution of time seizing per day [Fig. 5(f); $p = 0.0090$, and 0.0024, respectively, Kolmogorov-Smirnov test; for EGFR/ErbB-2 inhibitor, n = 6, from 2 animals; for cFMS inhibitor, n = 5, from 2 animals] and number of seizures per day [Fig. 5(g); $p = 0.0106$, and 0.0050, respectively]. Time seizing per day and number of seizures per day were normalized to the average time seizing and average number of seizures per day of vehicle-treated control cultures, respectively. Normalized cumulative time seizing and number of seizures, as well as p values of Kolmogorov-Smirnov tests of time seizing per day and number of seizures per day of all screened inhibitors were listed in Supplementary Table SII.

III. Discussion

In standard MEA designs, an insulation layer is required to confine the active area of electrodes in order to prevent signal dissipation and increase detection sensitivity. The most used insulation types are silicon dioxide, silicon nitride, and SU-8 [40]–[43]. Silicon dioxide and silicon nitride require chemical vapor deposition (CVD) and etching process for electrode opening. SU-8 layer is spin coated to the device, and then electrodes are exposed by photolithography. We were able to simplify the MEA design by excluding the insulation process to make the device cheaper and easier to fabricate. The SNR of large strip electrodes was only 20% lower than that of point electrodes for the purpose of detecting epileptiform activity. Since seizure signal detected by μflow-MEA electrodes was more than 20 times higher than the noise [Fig. 3(d)], this did not affect the accuracy of detection and quantification of seizure-like activity.

Phenytoin experiment demonstrated that the organotypic hippocampal culture model of epilepsy was not affected by the device. It also demonstrated that integrated large-area electrodes could accurately detect seizure-like activity, as predicted by simulations, to give a precise evaluation of antiepileptic drug effect on the number and duration of seizure-like events. Interestingly, the cultures showed even higher seizure frequency after the phenytoin treatment termination [Fig. 4(e), (f)]. This might be due to the long timescale (20 hours) of this microfluidic perfusion based wash-in and wash-out experiment. Seizure frequency and load progressively increase during epileptogenesis in organotypic hippocampal cultures, and increase in seizure frequency after phenytoin wash-out may reflect the natural progression of epilepsy in this model. Our results suggest that phenytoin cannot prevent epilepsy progression in this model, which agrees with previous observations [3]. Measurement of lactate and LDH production was carried out by sampling culture medium and utilizing standard plate reader to measure concentrations of these molecules. This technique is high-

throughput and enables rapid analysis of drug effects on biomarkers of epileptogenesis. However, lactate and LDH levels do not directly represent seizures and cell death: lactate is a byproduct of cellular metabolism and depends on the number of surviving neurons in the culture. Thus, analysis of cell death via LDH assay is necessary to interpret lactate level as a marker of seizure-like activity. However, LDH assay cannot reflect the cell death when apoptotic cells degrade without releasing LDH into culture supernatant [44]. Candidate drugs might have unpredictable effects on cell metabolism and survival, which would complicate the interpretation of lactate and LDH data. In contrast, continuous electrical recordings provide direct measurement of electrographic seizures, allowing more accurate assessment of drug efficacy. In Stage I, several inhibitors significantly decreased lactate and LDH productions, indicating that these RTKs may participate in epileptogenesis [Fig. 5(a), Supplementary Table SI]. However, chronic electrical assay confirmed only EGFR/ErbB-2 inhibitor and cFMS inhibitor to have significant antiepileptic effect in organotypic hippocampal culture model of epilepsy [Fig. 5(c)–(g), Supplementary Table SII]. Thus, some of the ‘hits’ found with lactate and LDH assays were false positives and probably occurred due to effects of inhibitors on cellular metabolism or survival, but not on seizures. Interestingly, no false negatives (drugs that were not effective in lactate/LDH assays, but effective in μflow-MEA assay) were found. These results confirm the utility of lactate and LDH assays as a first stage high-throughput biomarker assay of epileptogenesis, but also imply that it is important to use chronic electrical assay to remove false positives from biomarker screen results. High number of potential hits identified with biomarkers underscores the need for a chronic electrical assay with a reasonable throughput, such as μflow-MEA, in the antiepileptic drug discovery pipeline.

GW-2580, the cFMS inhibitor we used in this work, has been reported to also inhibit Trk receptors [45]. It is important to note that conditional deletion or inhibition of TrkB kinase have been reported to attenuate or eliminate seizures in animal models of epilepsy [46]–[50]. Therefore, there is likelihood that the antiepileptic effect we observed with cFMS inhibitor is due to its non-specific inhibition of Trk kinases. Regardless of the mechanism, the high effectiveness of GW-2580 in organotypic hippocampal culture model of epilepsy demonstrates the potential of this small molecule inhibitor for development as an antiepileptic drug. To the best of our knowledge, antiepileptic effects of EGFR/ErbB-2 inhibition have not been previously reported for chronic epilepsy, and dual inhibition of these RTKs may be a new target for antiepileptic drug development. However, a different EGFR/ErbB-2/ErbB-4 inhibitor did not show significant results, suggesting that inhibitor non-specificity may be responsible.

The system described in this work represents a single unit of the scalable epileptogenesis assay platform: 12 cultures on 2 μflow-MEA chips, recorded by 16 channel electrophysiology station to test 3 drug-treated conditions and a vehicle-treated control, with n = 3 cultures each condition. Placement of the drug-treated and control groups onto the same chip lowered experimental variability of the screening platform. This system can be easily scaled up through addition of more units to increase the throughput of drug discovery.

IV. Conclusion

We developed a hybrid μflow-MEA technology for scalable chronic electrical assay of epileptogenesis in organotypic hippocampal culture model. The simplified MEA electrode design enabled fabrication of a cost-effective device without compromising the sensitive detection of seizure-like activity. μflow-MEA based chronic electrical screening of inhibitors of hippocampal RTKs validated the results of a biomarker-based assay and identified inhibitors with antiepileptic effects. This epilepsy-on-a-chip screening platform provides the means to rapidly dissect complex signaling pathways involved in epileptogenesis, paving the way for high-throughput antiepileptic drug discovery.

V. Materials and Methods

A. Device fabrication

Glass slides (2 × 2 inch, Fisher Scientific) were cleaned in Piranha solution. Metal pattern was defined with negative lift-off process (AZ nLOF 2070, MicroChem). Titanium (50 nm) and gold (200 nm) were deposited with e-beam evaporator. Culture wells and microfluidic networks were fabricated in 100 μm thick PDMS films as previously described [19]. PDMS film was then attached to the MEA chip through oxygen plasma bonding, with electrodes centered in culture wells. Then 1.5 mm thick PDMS reservoir (8 mm × 25 mm inner area) and 2 mm thick input tubing stands (5 mm × 5 mm) were bonded to PDMS membrane. Tubing stand through-hole (0.1 mm diameter) was centered on the punctured fluid inlet. Steps of device fabrication and assembly are shown in Supplementary Fig. S1. To make a vacuum outlet that removes waste medium from the reservoir, a 1 mm long glass capillary tube was glued to a small piece of glass slide attached to the end of the reservoir. The integrated device was then autoclaved for sterilization before culturing.

B. Field potential simulation

Field potentials were simulated using COMSOL-Multiphysics (COMSOL Inc.). The 3D model geometry included the culture well, current source model of multiunit activity and seizures, and 2D recoding electrodes. Insulating boundary conditions were assigned to the circumference and the floor of the culture well, and the air-medium interface. The conductivity of the slice culture and medium were set as 0.3 S/m and 1.5 S/m, respectively, to match reported conductivity of brain tissue and artificial cerebrospinal fluid (aCSF) [51]–[53]. The maximum current source density was set at 4×10^4 A/m^3, when 100% neurons firing simultaneously. This value was estimated by multiplying synaptic current amplitude (200 pA, based on reported amplitude of evoked and spontaneous postsynaptic currents in epileptic hippocampal slice [54]–[57]) by neuron density in pyramidal layer in organotypic hippocampal slice (2×10^5/mm^3, based on our previous cell counting results [4]). The current dipole model of multiunit activity was represented by two spheres with radius = 20 μm, which contains around 7 neurons, and center-to-center distance = 200 μm, which is the approximate distance between geometric centers of soma and dendrites [Supplementary Fig. S3(a)]. The current source density was set to the maximum value. In the current source model of seizure-like activity, current source densities were set to the maximum value in *p*, *CA3p* and *lm* layers and 25% of maximum value in *g* layer. The lower current source density

in *g* layer is due to the granule cell dispersion during culturing. The compact lamination of granule cell bodies is lost [Fig. 2(a)], which compromises the bipolarity of DG cells [58].

C. Preparation of organotypic cultures

Hippocampi were dissected from postnatal day 7–8 Sprague-Dawley rat pups (Charles River Laboratories), and cut into 350 μm slices on a McIlwain tissue chopper (Mickle Laboratory Eng. Co., Surrey, United Kingdom). For experiments in stage I, cultures were created and maintained as described earlier [7]. Briefly, slices were placed onto poly-D-lysine (PDL, Sigma-Aldrich) coated 6-well tissue culture plates. Cultures were maintained in serum-free NeurobasalA/B27 medium containing 0.5 mM glutaMAX (Invitrogen) and 30 mg/L gentamicin (Invitrogen) and incubated at 37 °C in 5% CO2 on a rocking platform. Medium was changed twice a week. For experiments in stage II, slices were placed in the PDL coated mini culture wells of μflow-MEA device and were gravity-fed with the same medium from a syringe tube at the rate of 1 ml/day per culture in the same type incubator. All animal use protocols were approved by the Institution Animal Care and Use Committee (IACUC) at Lehigh University and were conducted in accordance with the United States Public Health Service Policy on Humane Care and Use of Laboratory Animals.

D. Lactate and lactate dehydrogenase (LDH) assays

Lactate and lactate dehydrogenase (LDH) measurements have been used to evaluate antiepileptic drug efficacy in organotypic cultures, since their concentrations in the spent culture medium were found to be correlated with seizure-like activity and seizure-dependent cell death, respectively [3], [6], [7]. Culture supernatant was collected during medium changes. Lactate and LDH concentrations in the supernatant were determined by using kits (Eton Bioscience and Roche Diagnostics, respectively) according to manufacturers' protocols. Lactate concentrations were calculated relative to known lactate standards, while LDH concentrations were normalized to the 0 – 3 days in vitro (DIV) average of LDH concentration in control culture supernatant.

E. Drug application and screens

Phenytoin was dissolved in dimethylsulfoxide (DMSO), and added to the culture medium at 100 ɜM concentration. Phenytoin was applied when consistent seizure-like activity was observed. Cultures were perfused by medium with phenytoin for 10 hours, then switched back to normal medium perfusion. Electrical recordings before, during and after drug perfusion were analyzed to evaluate the drug efficacy.

Cultures from the same animal were organized into four experimental groups to test three drugs with a vehicle-treated control (n = 3 cultures each condition). All inhibitors were dissolved in DMSO and applied to cultures starting on 3 DIV. Control cultures were treated with 0.1% DMSO as vehicle. Toxicity pre-screen (0–7 DIV) was conducted by morphology analysis and measurement of LDH on 7 DIV. Cultures showing either unhealthy morphology (detachment from the substrate, darkness, or indistinct neural layer) or significantly higher LDH than control were deemed toxic and a lower concentration of applied drug was retested until the maximum nontoxic concentration was identified. The maximum nontoxic concentration of each drug were then applied in two stage chronic screens. In Stage I,

culture supernatant was collected on 3, 7, 10, 14, 17 and 21 DIV and seizure-like activity and cell death were measured by lactate and LDH assay, respectively. In Stage II, cultures were perfused by culture medium with drugs from 3 DIV to 14 DIV. Chronic electrical recordings were then analyzed to evaluate drug efficacy.

F. Immunohistochemistry

NeuN antibody is a marker for neurons that specifically recognizes DNA-binding, neuron-specific protein NeuN. Cultures were washed in phosphate-buffered saline (PBS), fixed for 2 h in 4% paraformaldehyde, permeabilized in 0.3% Triton X-100 (Sigma-Aldrich) in PBS for 2 h, blocked with 10% goat serum in PBS for 1 h, and then incubated for 24 h in 1:100 NeuN at +4 °C on a shaker. Z-stack images were collected on confocal microscope (Zeiss LSM 510 META, Germany) with 5x and 40x objectives. Z-stack layers were separated by 1 μm, and slices were imaged over their total depth. Images were then processed in Fiji (ImageJ) [59]. Neurons in CA1 and CA3 pyramidal layers were quantified with a counting algorithm modified from existing “3D watershed technique” for counting cell nuclei (ImageJ macro developed by [60]).

G. Electrical recordings, stimulation and data analysis

Electrical stimulation (artificial signal for electrode performance evaluation) was delivered via 5 μA, 200 msec biphasic pulses (Model 2300, A-M Systems) to a bipolar electrode constructed from twisted insulated tungsten microwires (0.002”/0.004” conductor/insulator diameter, A-M Systems). Point recording electrodes were constructed from the same wire. Electrical recordings of neural activity were carried out by connecting the electrode contact pads on MEA to a 16-channel extracellular amplifier with high impedance head stage (3600, A-M Systems). Signals were digitized with a multiple-channel digital acquisition board (Measurement Computing). Sampling rate was 200 Hz per channel. Data were recorded with dClamp software (see Acknowledgements), and analyzed with Matlab (Mathworks). SNR was calculated from 1 min epoch of seizure-like event versus 1 min epoch of baseline (n = 6 electrodes). Electrographic seizures were defined as paroxysmal events (with significantly larger amplitudes than background population activity) that occurred for at least 10 seconds with event frequency of at least 2 Hz. A data binning algorithm was developed for automated quantification of seizure-like activity in chronic recordings. Color raster plots were created by binning the data at 0.5 s and calculating the number of super-threshold bins (represent paroxysmal events) per 10 seconds sliding window. Threshold was set at 20 ~ 45 μV, above the background non-paroxysmal activity in each recording channel.

H. Statistical Methods

We used Student’s *t* test for two-variable comparisons, one-way ANOVA with Holm-Sidak post hoc analysis for multiple variable comparisons, and Kolmogorov-Smirnov test for cumulative distribution analysis. Number of samples n refers to the number of cultures.

Supplementary Material

Refer to Web version on PubMed Central for supplementary material.

Acknowledgment

The authors would like to thank the Pediatric Epilepsy Research Lab at MGH, and in particular Waldemar (Waldi) Swiercz and PI Kevin J. Staley for kindly providing dClamp software.

This work was supported by NIH/NINDS grant R21/R33NS088358. The content is solely the responsibility of the authors and does not necessarily represent the official views of the National Institutes of Health.

References

[1]. Pitkänen A et al., “Epileptogenesis,” Cold Spring Harb. Perspect. Med, vol. 5, no. 10, p. a022822, Oct. 2015. [PubMed: 26385090]

[2]. Dyhrfjeld-Johnsen J et al., “Interictal spikes precede ictal discharges in an organotypic hippocampal slice culture model of epileptogenesis,” J. Clin. Neurophysiol, vol. 27, no. 6, pp. 418–424, 2010. [PubMed: 21076333]

[3]. Berdichevsky Y et al., “Interictal spikes, seizures and ictal cell death are not necessary for post-traumatic epileptogenesis in vitro,” Neurobiol. Dis, vol. 45, no. 2, pp. 774–785, 2012. [PubMed: 22115940]

[4]. Liu J et al., “Epileptogenesis in organotypic hippocampal cultures has limited dependence on culture medium composition,” PLOS ONE, vol. 12, no. 2, p. e0172677, Feb. 2017. [PubMed: 28225808]

[5]. Lillis KP et al., “Evolution of network synchronization during early epileptogenesis parallels synaptic circuit alterations,” J. Neurosci, vol. 35, no. 27, pp. 9920–9934, 2015. [PubMed: 26156993]

[6]. Berdichevsky Y et al., “PI3K-Akt signaling activates mTOR-mediated epileptogenesis in organotypic hippocampal culture model of post-traumatic epilepsy,” J. Neurosci, vol. 33, no. 21, pp. 9056–9067, 2013. [PubMed: 23699517]

[7]. Berdichevsky Y et al., “Staged anticonvulsant screening for chronic epilepsy,” Ann. Clin. Transl. Neurol, vol. 3, no. 12, pp. 908–923, Dec. 2016. [PubMed: 28097203]

[8]. Park K-I et al., “What elements of the inflammatory system are necessary for epileptogenesis in vitro?,” eneuro, vol. 2, no. 2, p. ENEURO 0027–14.2015, 2015.

[9]. Dzhala V and Staley KJ, “Acute and Chronic Efficacy of Bumetanide in an in vitro Model of Posttraumatic Epileptogenesis,” CNS Neurosci. Ther, vol. 21, no. 2, pp. 173–180, 2015. [PubMed: 25495911]

[10]. Gutiérrez R and Heinemann U, “Synaptic reorganization in explanted cultures of rat hippocampus,” Brain Res, vol. 815, no. 2, pp. 304–316, 1999. [PubMed: 9878801]

[11]. Egert U et al., “A novel organotypic long-term culture of the rat hippocampus on substrate-integrated multielectrode arrays,” Brain Res. Protoc, vol. 2, no. 4, pp. 229–242, 1998.

[12]. Corner M et al., “Physiological effects of sustained blockade of excitatory synaptic transmission on spontaneously active developing neuronal networks—an inquiry into the reciprocal linkage between intrinsic biorhythms and neuroplasticity in early ontogeny,” Neurosci. Biobehav. Rev, vol. 26, no. 2, pp. 127–185, 2002. [PubMed: 11856557]

[13]. Beggs JM, “Neuronal Avalanches Are Diverse and Precise Activity Patterns That Are Stable for Many Hours in Cortical Slice Cultures,” J. Neurosci, vol. 24, no. 22, pp. 5216–5229, 2004. [PubMed: 15175392]

[14]. Johnson HA and Buonomano DV, “Development and Plasticity of Spontaneous Activity and Up States in Cortical Organotypic Slices,” J. Neurosci, vol. 27, no. 22, pp. 5915–5925, 2007. [PubMed: 17537962]

[15]. Hofmann F et al., “Functional re-establishment of the perforant pathway in organotypic co-cultures on microelectrode arrays,” Brain Res, vol. 1017, no. 1–2, pp. 184–196, 8.

[16]. Hofmann F and Bading H, “Long term recordings with microelectrode arrays: Studies of transcription-dependent neuronal plasticity and axonal regeneration,” J. Physiol.-Paris, vol. 99, no. 2–3, pp. 125–132,3. [PubMed: 16442786]

[17]. Gong W. Long-term, high-spatiotemporal resolution recording from cultured organotypic slices with high-density microelectrode arrays. presented at the 2015 Transducers - 2015 18th International Conference on Solid-State Sensors, Actuators and Microsystems (TRANSDUCERS); 2015. 1037–1040.

[18]. Killian NJ et al., "A Device for Long-Term Perfusion, Imaging, and Electrical Interfacing of Brain Tissue In vitro," Front. Neurosci, vol. 10, p. 135, received 2016. [PubMed: 27065793]

[19]. Liu J et al., "Perfused drop microfluidic device for brain slice culture-based drug discovery," Biomed Microdevices, vol. 18, no. 3, p. 46, Jun. 2016. [PubMed: 27194028]

[20]. Lein ES et al., "Genome-wide atlas of gene expression in the adult mouse brain," Nature, vol. 445, no. 7124, p. 168, Jan. 2007. [PubMed: 17151600]

[21]. Liu B et al., "Epidermal Growth Factor Receptor Activation: An Upstream Signal for Transition of Quiescent Astrocytes into Reactive Astrocytes after Neural Injury," J. Neurosci, vol. 26, no. 28, pp. 7532–7540, Jul. 2006. [PubMed: 16837601]

[22]. Leadbeater WE et al., "Intracellular trafficking in neurones and glia of fibroblast growth factor-2, fibroblast growth factor receptor 1 and heparan sulphate proteoglycans in the injured adult rat cerebral cortex," J. Neurochem, vol. 96, no. 4, pp. 1189–1200, Feb. 2006. [PubMed: 16417571]

[23]. Nagayama T et al., "Post-ischemic delayed expression of hepatocyte growth factor and c-Met in mouse brain following focal cerebral ischemia," Brain Res, vol. 999, no. 2, pp. 155–166, Mar. 2004. [PubMed: 14759494]

[24]. Schäbitz W-R et al., "A Neuroprotective Function for the Hematopoietic Protein Granulocyte-Macrophage Colony Stimulating Factor (GM-CSF)," J. Cereb. Blood Flow Metab, vol. 28, no. 1, pp. 29–43, Jan. 2008. [PubMed: 17457367]

[25]. Tokita Y et al., "Regulation of Neuregulin Expression in the Injured Rat Brain and Cultured Astrocytes," J. Neurosci, vol. 21, no. 4, pp. 1257–1264, Feb. 2001. [PubMed: 11160396]

[26]. Sköld MK et al., "VEGF and VEGF Receptor Expression after Experimental Brain Contusion in Rat," J. Neurotrauma, vol. 22, no. 3, pp. 353–367, Mar. 2005. [PubMed: 15785231]

[27]. Helmy A et al., "The Cytokine Response to Human Traumatic Brain Injury: Temporal Profiles and Evidence for Cerebral Parenchymal Production," J. Cereb. Blood Flow Metab, vol. 31, no. 2, pp. 658–670, Feb. 2011. [PubMed: 20717122]

[28]. Pitkänen A and Lukasiuk K, "Mechanisms of epileptogenesis and potential treatment targets," Lancet Neurol, vol. 10, no. 2, pp. 173–186, 2011. [PubMed: 21256455]

[29]. Loscher W and Brandt C, "Prevention or Modification of Epileptogenesis after Brain Insults: Experimental Approaches and Translational Research," Pharmacol. Rev, vol. 62, no. 4, pp. 668–700, 2010. [PubMed: 21079040]

[30]. Buzsáki G et al. "The origin of extracellular fields and currents—EEG, ECoG, LFP and spikes," Nat. Rev. Neurosci, vol. 13, no. 6, pp. 407–420, 2012. [PubMed: 22595786]

[31]. Buzsáki G, "Hippocampal sharp wave-ripple: A cognitive biomarker for episodic memory and planning," Hippocampus, vol. 25, no. 10, pp. 1073–1188, Oct. 2015. [PubMed: 26135716]

[32]. Wheeler BC and Novak JL, "Current Source Density Estimation Using Microelectrode Array Data from the Hippocampal Slice Preparation," IEEE Trans. Biomed. Eng, vol. BME-33, no. 12, pp. 1204–1212, Dec. 1986.

[33]. Gonzalez-Sulser A et al., "The 4-aminopyridine in vitro epilepsy model analyzed with a perforated multi-electrode array," Neuropharmacology, vol. 60, no. 7, pp. 1142–1153, Jun. 2011. [PubMed: 20955719]

[34]. Tsintsadze V et al., "Ontogeny of kainate-induced gamma oscillations in the rat CA3 hippocampus in vitro," Front. Cell. Neurosci, vol. 9, May 2015.

[35]. Hájos N et al., "Maintaining network activity in submerged hippocampal slices: importance of oxygen supply," Eur. J. Neurosci, vol. 29, no. 2, pp. 319–327, Jan. 2009. [PubMed: 19200237]

[36]. Hájos N and Mody I, "Establishing a physiological environment for visualized in vitro brain slice recordings by increasing oxygen supply and modifying aCSF content," J. Neurosci. Methods, vol. 183, no. 2, pp. 107–113, 2009. [PubMed: 19524611]

[37]. Hill AJ et al., "Development of multi-electrode array screening for anticonvulsants in acute rat brain slices," J. Neurosci. Methods, vol. 185, no. 2, pp. 246–256, 1. [PubMed: 19836417]

[38]. Berdichevsky Y et al., “Microfluidics and multielectrode array-compatible organotypic slice culture method,” J. Neurosci. Methods, vol. 178, no. 1, pp. 59–64, 2009. [PubMed: 19100768]

[39]. Ferrea E et al., “Large-scale, high-resolution electrophysiological imaging of field potentials in brain slices with microelectronic multielectrode arrays,” Front. Neural Circuits, vol. 6, Nov. 2012.

[40]. Bonnauron M et al., “High aspect ratio diamond microelectrode array for neuronal activity measurements,” Diam. Relat. Mater, vol. 17, no. 7, pp. 1399–1404, Jul. 2008.

[41]. Berdondini L et al., “A microelectrode array (MEA) integrated with clustering structures for investigating in vitro neurodynamics in confined interconnected sub-populations of neurons,” Sens. Actuators B Chem, vol. 114, no. 1, pp. 530–541, Mar. 2006.

[42]. Heuschkel MO et al., “A three-dimensional multi-electrode array for multi-site stimulation and recording in acute brain slices,” J. Neurosci. Methods, vol. 114, no. 2, pp. 135–148, 2002. [PubMed: 11856564]

[43]. Seker E et al., “The fabrication of low-impedance nanoporous gold multiple-electrode arrays for neural electrophysiology studies,” Nanotechnology, vol. 21, no. 12, p. 125504, 2010. [PubMed: 20203356]

[44]. Bonfoco E et al., “Apoptosis and necrosis: two distinct events induced, respectively, by mild and intense insults with N-methyl-D-aspartate or nitric oxide/superoxide in cortical cell cultures,” Proc. Natl. Acad. Sci. U. S. A, vol. 92, no. 16, pp. 7162–7166, 1995. [PubMed: 7638161]

[45]. Davis MI et al., “Comprehensive analysis of kinase inhibitor selectivity,” Nat. Biotechnol, vol. 29, no. 11, pp. 1046–1051, Oct. 2011. [PubMed: 22037378]

[46]. He X-P et al., “Conditional deletion of TrkB but not BDNF prevents epileptogenesis in the kindling model,” Neuron, vol. 43, no. 1, pp. 31–42, Jul. 2004. [PubMed: 15233915]

[47]. Kotloski R and McNamara JO, “Reduction of TrkB expression de novo in the adult mouse impairs epileptogenesis in the kindling model,” Hippocampus, vol. 20, no. 6, pp. 713–723, Jun. 2010. [PubMed: 19603519]

[48]. Liu G et al., “Transient inhibition of TrkB kinase after status epilepticus prevents development of temporal lobe epilepsy,” Neuron, vol. 79, no. 1, pp. 31–38, 2013. [PubMed: 23790754]

[49]. Liu G et al., “Antiseizure effects of TrkB kinase inhibition,” Epilepsia, vol. 55, no. 8, pp. 1264–1273, Aug. 2014. [PubMed: 24903749]

[50]. Gu B et al., “A Peptide Uncoupling BDNF Receptor TrkB from Phospholipase Cΰ1 Prevents Epilepsy Induced by Status Epilepticus,” Neuron, vol. 88, no. 3, pp. 484–491, Nov. 2015. [PubMed: 26481038]

[51]. Nunez PL and Srinivasan R, Electric fields of the brain: the neurophysics of EEG. Oxford University Press, USA, 2006.

[52]. Logothetis NK et al., “In Vivo Measurement of Cortical Impedance Spectrum in Monkeys: Implications for Signal Propagation,” Neuron, vol. 55, no. 5, pp. 809–823, Sep. 2007. [PubMed: 17785187]

[53]. Miceli S et al., “Impedance Spectrum in Cortical Tissue: Implications for Propagation of LFP Signals on the Microscopic Level,” eNeuro, vol. 4, no. 1, Feb. 2017.

[54]. Simmons ML et al., “Spontaneous Excitatory Currents and ţ-Opioid Receptor Inhibition in Dentate Gyrus Are Increased in the Rat Pilocarpine Model of Temporal Lobe Epilepsy,” J. Neurophysiol, vol. 78, no. 4, pp. 1860–1868, Oct. 1997. [PubMed: 9325355]

[55]. Okazaki MM et al., “Recurrent Mossy Fiber Pathway in Rat Dentate Gyrus: Synaptic Currents Evoked in Presence and Absence of Seizure-Induced Growth,” J. Neurophysiol, vol. 81, no. 4, pp. 1645–1660, Apr. 1999. [PubMed: 10200201]

[56]. Prince DA et al., “Epilepsy following cortical injury: Cellular and molecular mechanisms as targets for potential prophylaxis,” Epilepsia, vol. 50, pp. 30–40, Feb. 2009.

[57]. Kovács R et al., “Endogenous Nitric Oxide Is a Key Promoting Factor for Initiation of Seizure-Like Events in Hippocampal and Entorhinal Cortex Slices,” J. Neurosci, vol. 29, no. 26, pp. 8565–8577, Jul. 2009. [PubMed: 19571147]

[58]. Sloviter RS et al., “Abnormal dentate gyrus network circuitry in temporal lobe epilepsy,” in Jasper’s Basic Mechanisms of the Epilepsies, 4th ed., Noebels JL, Avoli M, Rogawski MA,

Olsen RW, and Delgado-Escueta AV, Eds. Bethesda (MD): National Center for Biotechnology Information (US), 2012.

[59]. Schindelin J et al., "Fiji: an open-source platform for biological-image analysis," Nat. Methods, vol. 9, no. 7, pp. 676–682, 2012. [PubMed: 22743772]

[60]. Bindokas V, 17-9-2014 [Online]. Available: https://digital.bsd.uchicago.edu/%5Cimagej_macros.html.

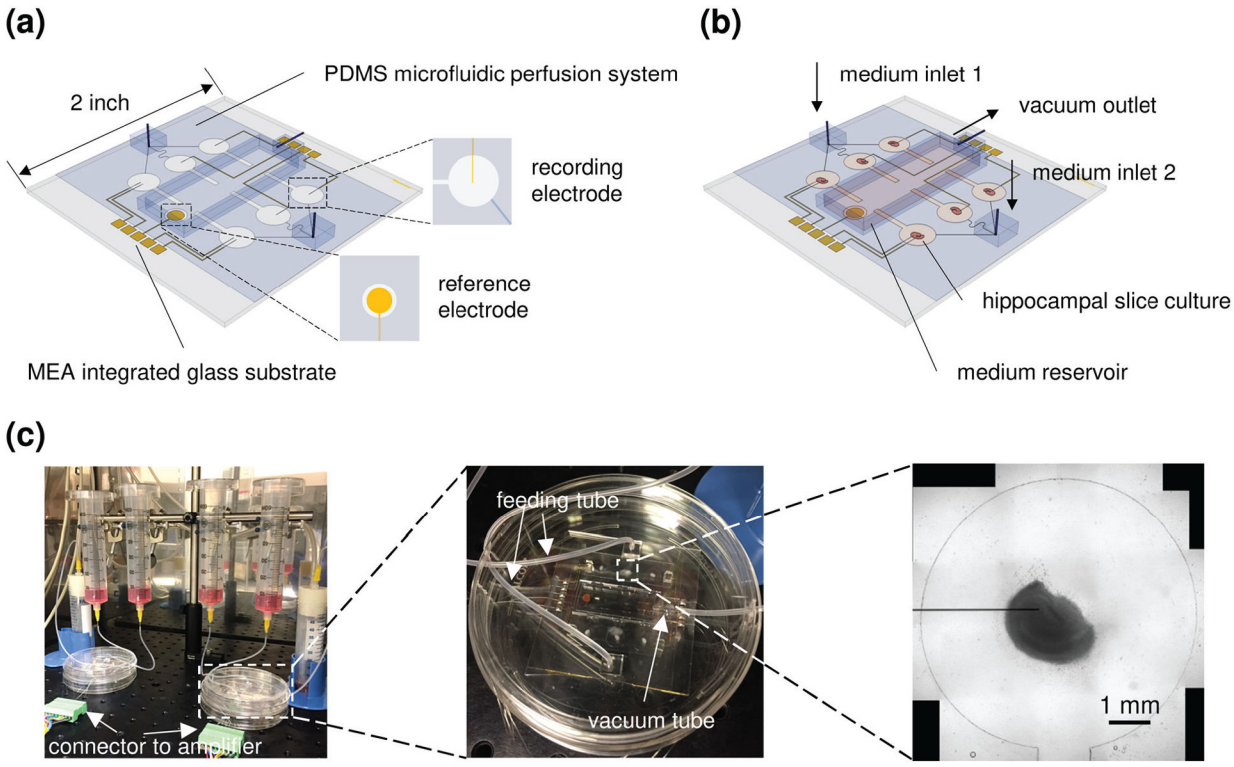

Fig. 1.

Integrated μflow-MEA system for chronic recording in multiple hippocampal slice cultures. (a) Schematic representation of the μflow-MEA chip. (b) Schematic of a device in operation, with hippocampal slices loaded and perfused by medium through microchannels, and the waste medium in the reservoir was removed via the vacuum outlet. (c) Fully assembled system prototype, with a photo of the device, and a brightfield image of a hippocampal culture maintained in the mini well with one substrate-integrated strip electrode. Scale bar, 1 mm.

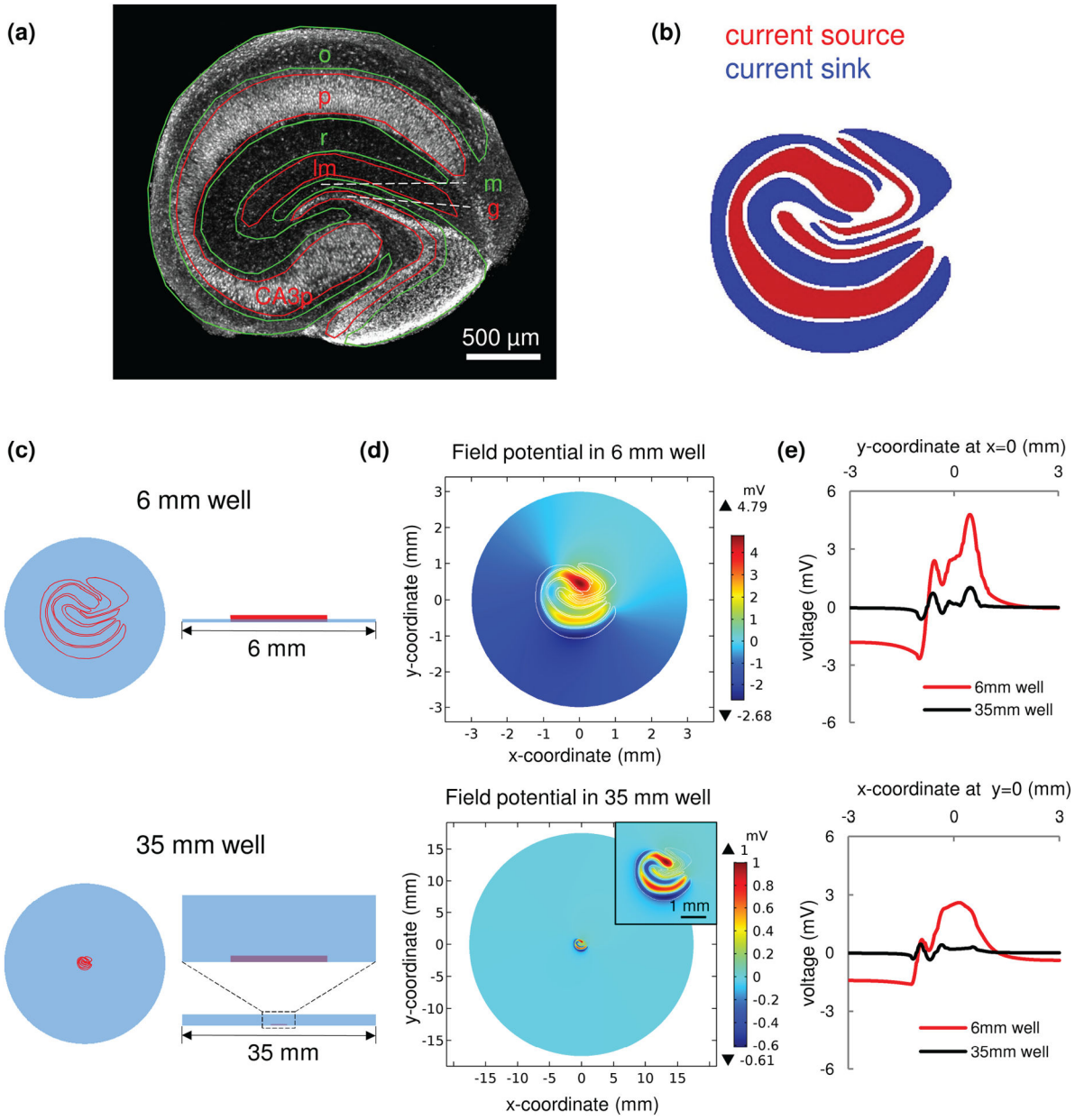

Fig. 2.

Simulation of the field potential generated by seizure-like activity. (a) Hippocampal slice anatomy. Red and green lines represent opposite polarity of current flow in each neural layer during synchronized synaptic transmission (when dendrite layers are receiving excitatory synaptic inputs: green, sink; red, source). Micrograph image is an organotypic hippocampal culture stained with antibody to NeuN – protein predominantly expressed in neuronal nuclei. (b) Current source pattern during seizure-like activity with whole hippocampal circuit synchronized (blue, sink; red, source). (c) Slice culture maintained in an interface mini well (top; diameter = 6 mm, fluid depth = 100 µm – same dimensions as in µflow-MEA device), and in a standard submerged dish (bottom; diameter = 35 mm, fluid depth = 2 mm). (d) Simulated field potential in mini well (top; white lines show the outline of neural layers),

and standard well (bottom). The insert shows hippocampal slice at higher magnification. Scale bar, 1 mm. (e) Field potential distribution along the x=0 (top) and y=0 (bottom) axis (red, mini well; black, standard well). The simulation results refer to the horizontal plane at the well floor. *o*, stratum oriens; *p*, pyramidal layer; *r*, stratum radiatum; *lm*, stratum lacunosum-moleculare; *m*, dentate molecular layer; *g*, granule cell layer; *CA3p*, pyramidal layer of CA3c subregion.

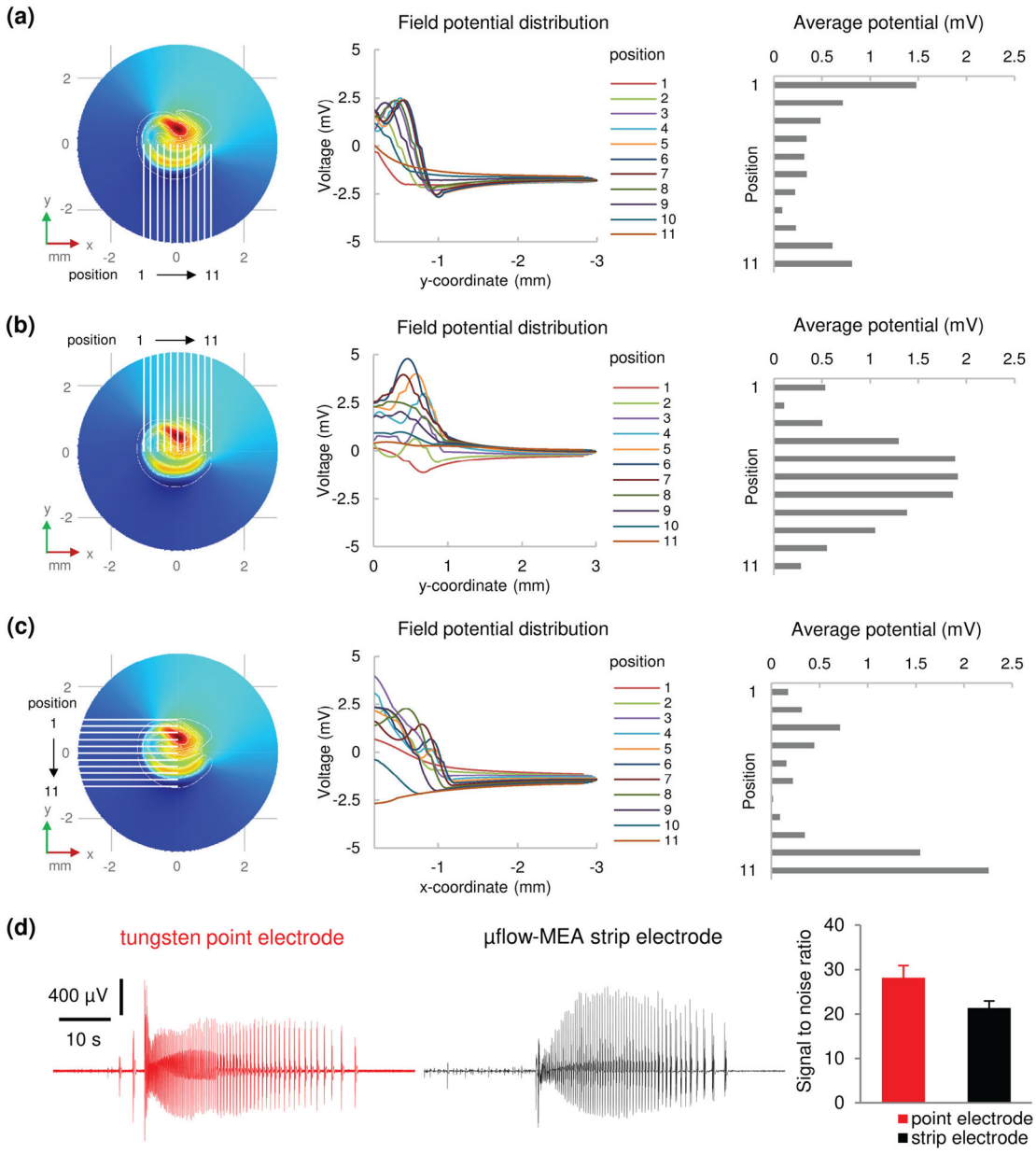

Fig. 3.

Field potentials due to seizure-like activity detected by large area strip electrodes. (a-c) Simulation results. (a) Left, electrodes recording from CA1 area (position 1 to 11 refers to x = −1 mm to x = 1 mm, with 0.2 mm interval). Middle, field potential distribution along each electrode. Right, average potential that is detected by each electrode. (b) Results of electrodes recording from CA3 and DG area. (c) Results of electrodes recording from CA3 and CA1 area (position 1 to 11 refers to y = 1 mm to y = −1 mm, with 0.2 mm interval). (d) Experimental recordings. Left: representative seizure-like events recorded by tungsten microelectrode (point electrode) and strip electrode. Scale bars as indicated in figure. Right: signal to noise ratio of point electrodes and strip electrodes. n = 6 electrodes for each type. Error bars indicate standard deviation (SD).

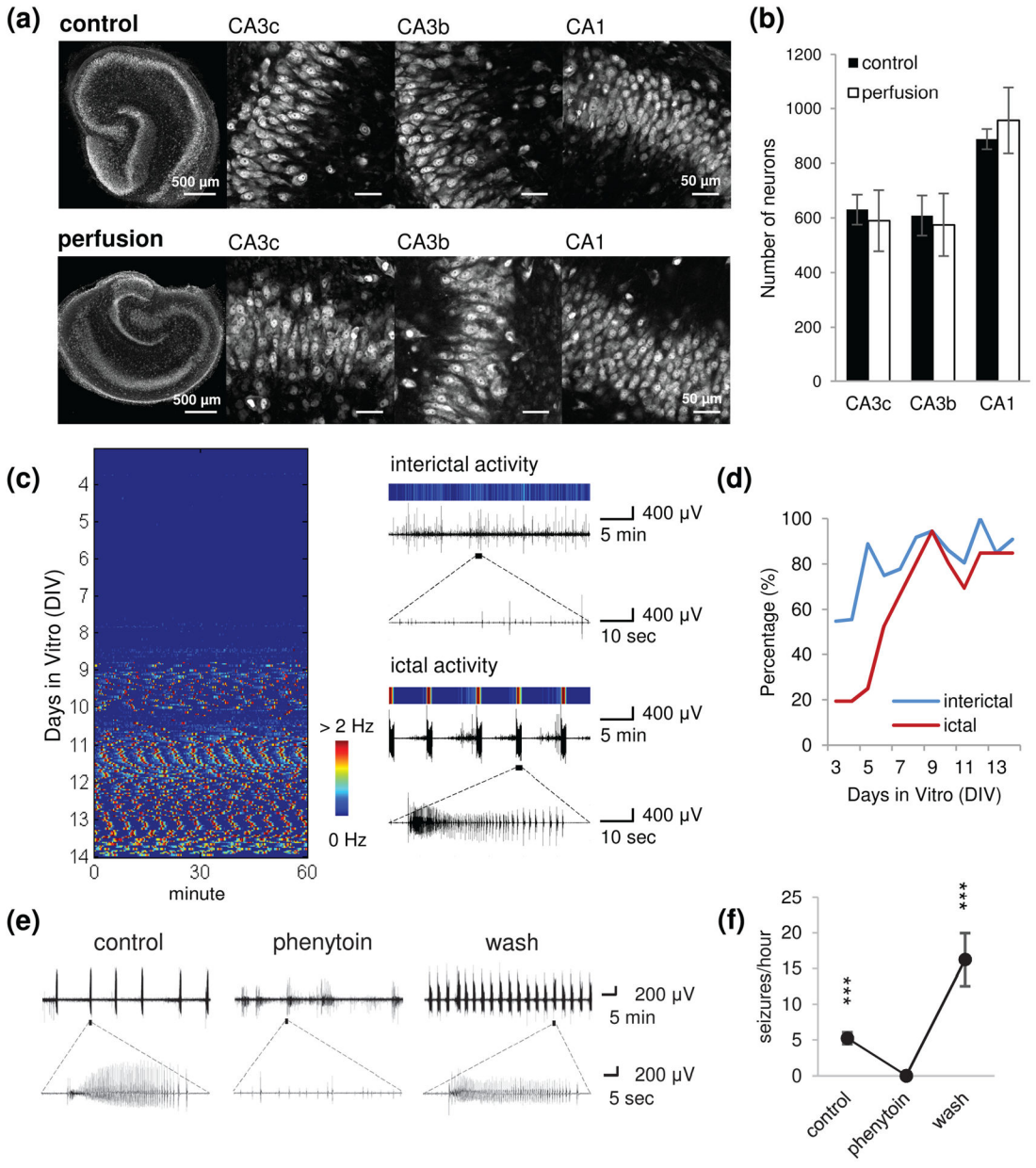

Fig. 4.

Epilepsy-on-a-chip model validation. (a) Representative confocal imaging of NeuN staining in control cultures (interface method) and perfused cultures (μflow-MEA) on 14 day in vitro (DIV), and high magnification images of CA3c, CA3b and CA1 regions. Scale bars as indicated in figure. (b) Neuron counts in CA3c, CA3b, and CA1. n = 9 each condition. (c) Left: representative raster plot of chronic recording from 4 to 14 DIV. Color corresponds to the frequency of paroxysmal events, with low frequency indicated by blue, and high frequency (seizures) indicated by red. Each horizontal line of the raster plot represents one hour of recording, with 24 lines per DIV. Right: the color map of interictal activity (top trace) and ictal activity (seizure, bottom trace). (d) Incidence of ictal and interictal activity as a percentage of cultures recorded on μflow-MEA, with age of culture. n = 36 cultures, from

10 animals. (e) Representative recordings for each time period (control, phenytoin treatment, wash). (f) Seizure frequency during each period. n = 3. Error bars indicate SD. Statistical significance is indicated as ***, representing $p < 0.001$.

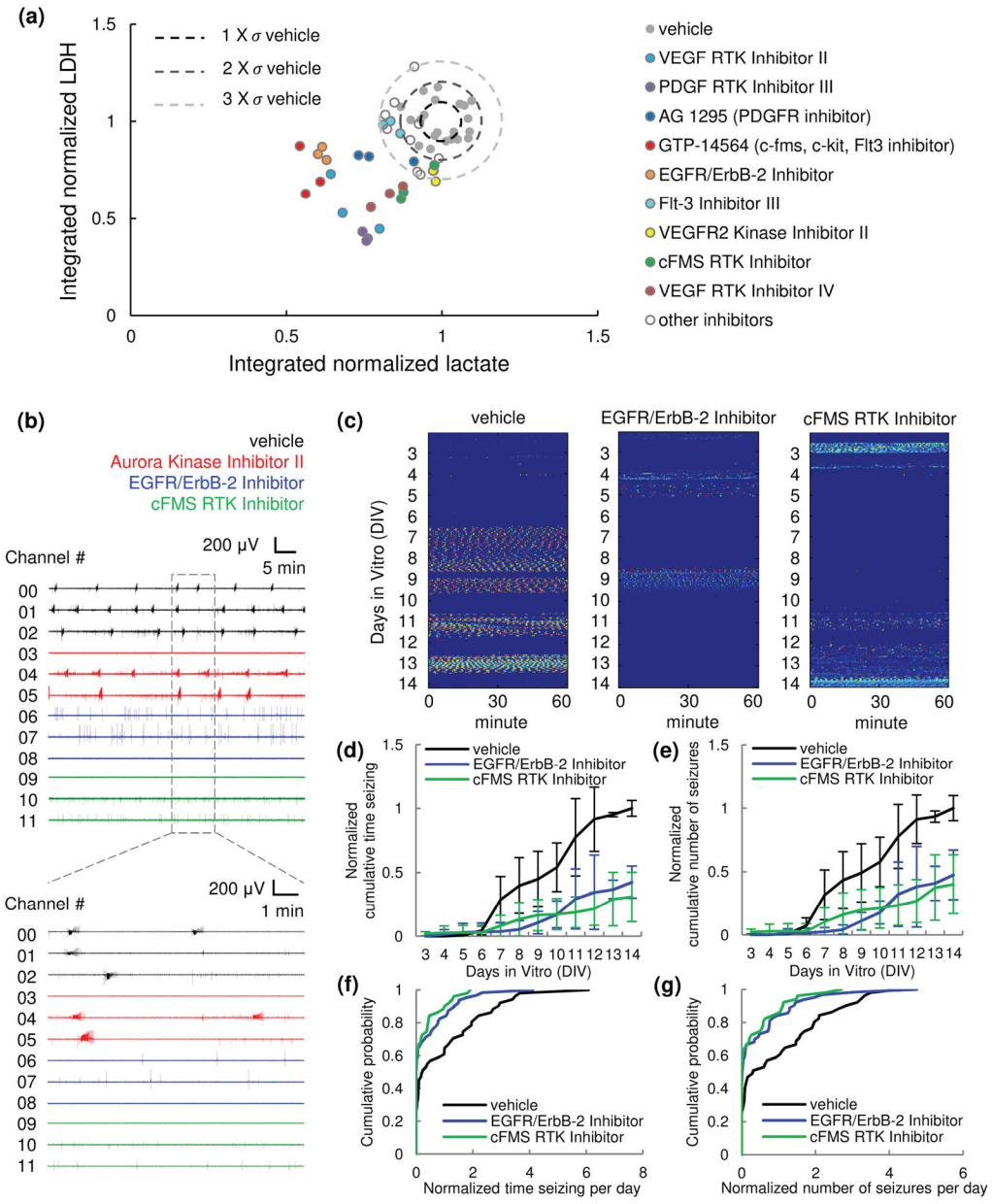

Fig. 5.

Chronic screen of receptor tyrosine kinase (RTK) inhibitors. (a) Stage I screen by biomarker (lactate and LDH) assay. Integrated lactate production (DIV3–14) versus integrated LDH production (DIV3–14) is plotted for 12 RTK inhibitors. Data represents values from individual cultures and was normalized to controls from the same animal. = standard deviation of integrated lactate (horizontal axis) and LDH (vertical axis) of controls. Drugs that showed strong reducing effect are highlighted. (b-g) Stage II screen by chronic electrical assay. (b) Representative 1 hour recording, showing parallel monitoring of epileptogenesis in 12 organotypic hippocampal cultures (black, vehicle; red, Aurora inhibitor II; blue, EGFR/ErbB-2 inhibitor; green, cFMS inhibitor). n = 3 cultures each condition, cultures are from the same animal. (c) Representative raster plots of chronic recordings of vehicle-treated

control, EGFR/ErbB-2 inhibitor-treated, and cFMS inhibitor-treated cultures. (d, e) Normalized cumulative time seizing and normalized cumulative number of seizures. Data was normalized to the total time seizing and total number of seizure of vehicle-treated controls from the same animal. For EGFR/ErbB-2 inhibitor, n = 6, from 2 animals. For cFMS inhibitor, n = 5, from 2 animals. Error bars indicate SD. (f, g) Cumulative distribution of normalized time seizing per day and normalized number of seizures per day. Data was normalized to the average time seizing per day and average number of seizure per day of vehicle-treated controls from the same animal.